



HAL
open science

Space Plasma Diagnostics and Spacecraft Charging. The Impact of Plasma Inhomogeneities on Mutual Impedance Experiments

L. Bucciantini, P. Henri, Gaëtan Wattieaux, F. Lavorenti, P. Dazzi, Xavier Vallières

► To cite this version:

L. Bucciantini, P. Henri, Gaëtan Wattieaux, F. Lavorenti, P. Dazzi, et al.. Space Plasma Diagnostics and Spacecraft Charging. The Impact of Plasma Inhomogeneities on Mutual Impedance Experiments. Journal of Geophysical Research Space Physics, 2023, 128, 10.1029/2023JA031534 . insu-04197021

HAL Id: insu-04197021

<https://insu.hal.science/insu-04197021v1>

Submitted on 9 Nov 2023

HAL is a multi-disciplinary open access archive for the deposit and dissemination of scientific research documents, whether they are published or not. The documents may come from teaching and research institutions in France or abroad, or from public or private research centers.

L'archive ouverte pluridisciplinaire **HAL**, est destinée au dépôt et à la diffusion de documents scientifiques de niveau recherche, publiés ou non, émanant des établissements d'enseignement et de recherche français ou étrangers, des laboratoires publics ou privés.



Distributed under a Creative Commons Attribution - NonCommercial - ShareAlike 4.0 International License



RESEARCH ARTICLE

10.1029/2023JA031534

Key Points:

- The locality of the plasma diagnostic of Mutual Impedance (MI) experiments is investigated for the first time
- Local inhomogeneities do not affect MI plasma density measurements but can impact the electron temperature diagnostic
- The locality of MI plasma diagnostic is investigated using 1D-1V cartesian Vlasov-Poisson numerical simulations

Correspondence to:

L. Bucciantini,
luca.bucciantini@cnrs.fr

Citation:

Bucciantini, L., Henri, P., Wattieaux, G., Lavorenti, F., Dazzi, P., & Vallières, X. (2023). Space plasma diagnostics and spacecraft charging. The impact of plasma inhomogeneities on mutual impedance experiments. *Journal of Geophysical Research: Space Physics*, 128, e2023JA031534. <https://doi.org/10.1029/2023JA031534>

Received 29 MAR 2023




Accepted 14 AUG 2023

The copyright line for this article was changed on 23 SEP 2023 after original online publication.

© 2023. The Authors.

This is an open access article under the terms of the [Creative Commons Attribution-NonCommercial-NoDerivs License](#), which permits use and distribution in any medium, provided the original work is properly cited, the use is non-commercial and no modifications or adaptations are made.

Space Plasma Diagnostics and Spacecraft Charging. The Impact of Plasma Inhomogeneities on Mutual Impedance Experiments

L. Bucciantini¹ , P. Henri^{1,2} , G. Wattieaux³, F. Lavorenti^{2,4}, P. Dazzi^{1,5} , and X. Vallières¹

¹Laboratoire de Physique et Chimie de l'Environnement et de l'Espace (LPC2E), CNRS, Université d'Orléans, Orléans, France, ²Laboratoire Lagrange, OCA, UCA, CNRS, Nice, France, ³Laboratoire Plasma et Conversion d'Energie (LAPLACE), CNRS, Université de Toulouse, Toulouse, France, ⁴Dipartimento di Fisica, Università di Pisa, Pisa, Italy, ⁵Laboratoire d'Études Spatiales et d'Instrumentation en Astrophysique (LESIA), Paris Observatory, Paris, France

Abstract Plasma diagnostic instruments are carried into space by satellites to measure in situ the properties of space plasmas. However, due to spacecraft charging, satellites perturb the surrounding plasma, that reacts by enveloping the platform and its instruments with a short scale, strongly inhomogeneous plasma region called plasma sheath. Such plasma sheath perturbs particles and electric field measurements performed onboard the satellite. Mutual Impedance (MI) experiments are a type of in situ diagnostic technique used in several space missions for the identification of the plasma density and the electron temperature. The technique is based on the electric coupling between emitting and receiving electric sensors embedded in the plasma to diagnose. Such sensors are surrounded by the plasma sheath, which is expected to affect the plasma response to MI emissions. In this context, we quantify for the first time the impact of the plasma sheath on the diagnostic performance of MI experiments. For this purpose, we use a full kinetic Vlasov-Poisson model to simulate numerically MI experiments in an inhomogeneous medium. For the first time, we explain the locality of MI measurements. We find that MI plasma density diagnostic are not affected by the plasma sheath ($dn/n < 10\%$). The experiment retrieves the density of the plasma unperturbed by the satellite's presence. The electron temperature diagnostic, instead, presents significant perturbations if the plasma sheath is ignored. To mitigate such electron temperature errors, the plasma sheath needs to be included in the analysis of MI measurements.

1. Introduction

In the context of space exploration, satellites carry scientific instruments to observe both in situ and remotely the properties of various parts of our solar system. Such observations rely on the assumption that the monitored properties are not perturbed by the presence of the satellites on which the monitoring instruments are installed. However, as a consequence of spacecraft-plasma interaction processes, satellites in space acquire an electric DC potential which is of the order of the plasma (DC) potential (Grard et al., 1983; Lai, 2012). The satellite's potential perturbs in multiple ways the characteristics of the local environment and, therefore, it can affect different types of in situ observations (Johansson et al., 2021). First, the electric potential gradient surrounding the satellite generates an electric field that affects both wave and particles measurements. In particular, electric field lines (Marchand et al., 2010) and particles trajectories (Bergman et al., 2020) are modified by the DC electric field of the satellite, resulting in perturbations of both electric field, particle and velocity distribution measurements performed onboard (Miyake & Usui, 2016). Second, the DC electric charge of the satellite is Debye shielded (i.e., neutralized) by the plasma, which forms strong small-scale (of the order of the Debye length) inhomogeneous plasma regions around the satellite platform. Such inhomogeneous regions are called plasma sheath (Allen, 2008; Laframboise, 1966; Riemann, 2008; Tonks & Langmuir, 1929). The plasma sheath is expected to modify the properties of plasma waves propagating from the satellite platform and, consequently, it is expected to impact plasma wave instruments. In this study, we focus on a particular type of electric experiment, called Mutual Impedance (MI) experiment. The objective of this study is to quantify the impact that plasma inhomogeneities have on MI diagnostic performance.

MI experiments are plasma diagnostic techniques used for the identification of the in situ plasma density and electron temperature. In the past, different versions of MI instruments were included in the scientific payload of space exploration missions targeting both near (e.g., the Earth and its ionosphere) (Bahnsen et al., 1988; Béghin & Debrie, 1972; Décréau et al., 1978; Grard, 1997; Pottelette & Storey, 1981; Pottelette et al., 1975; Storey

et al., 1969) and far (e.g., comet 67P/CG investigated by the ESA Rosetta mission (Taylor et al., 2017) carrying the RPC-MIP instrument) (Trotignon et al., 2007) objects of our solar system. Recently, new versions of MI instruments have been included in ongoing and future exploration missions, such as the ESA/JAXA mission BepiColombo (Benkhoff et al., 2021) (PWI-AM2P experiment) (Kasaba et al., 2020; Trotignon et al., 2006) that will investigate Mercury, the ESA mission JUICE (RPWI-MIME experiment) that will explore Jovian moons and the ESA mission Comet Interceptor (DFP-COMPLIMENT instrument) that will perform a multi-point fly by observation of a pristine comet entering the solar system for the first time (Snodgrass & Jones, 2019).

MI instruments consist of a set of emitting and receiving electric antennas. The emitting antennas excite the plasma with electric sinusoidal signals. Simultaneously to the emission, the receiving antennas measure the plasma fluctuations generated by the emitting sensors at the emission frequency. Such fluctuations are used for building MI spectra, which show resonant signatures in correspondence to characteristic frequencies of the probed plasma. The plasma density and electron temperature are identified from the position and shape of such resonant signatures, respectively (Décréau et al., 1978; Gilet et al., 2017; Storey et al., 1969; Wattiaux et al., 2020). MI spectra present one or multiple resonances, depending on the specific characteristics of the probed plasma. In the simplest case, corresponding to MI measurements obtained in an unmagnetized plasma with a single electron population and a fixed ion background, MI spectra present only one resonance. This resonance is located at the plasma frequency of the probed medium (ω_p). It follows that the frequencies associated to the position of the resonance are used to identify the plasma frequency and, therefore, the plasma density of the medium. In all, the plasma density is identified from collective oscillations of the electrons, triggered by the MI emitted signals exciting a sufficiently wide frequency band. The electron temperature, instead, is obtained from the analysis of the shape of the resonance detected on the MI spectra. Indeed, the shape of the resonance is strictly related to the Landau damping of the waves emitted by the MI instrument. As the plasma waves propagate from the MI emitting sensors to the receiving sensors, they get damped with a rate proportional to the derivative of the electron distribution function, calculated at the phase velocity of the emitted wave. Smaller phase velocities, associated to larger ratios of emitted frequency (ω) to plasma frequency ω/ω_p , are associated to stronger damping effects. In all, the MI electron temperature diagnostic is significantly dependent on the local damping of the emitted waves in the vicinity of MI sensors. Therefore, it strongly depends on the local characteristics of the plasma surrounding the MI sensors. As discussed in the following sections, this is believed to be the reason for the significant impact that the plasma sheath has on the MI electron temperature diagnostic.

In the case of typical space applications, different spurious electric signals generated in the surroundings of MI antennas are expected to affect MI measurements. The most significant sources of perturbation are: (i) electronic components (e.g., active electric instruments) installed onboard the satellite, (ii) the spacecraft platform, and (iii) the MI instrument itself.

- (i) Electronic components onboard the satellite emit electric signals which might affect MI measurements both directly, by being detected by MI receiving antennas, and indirectly, by modifying the plasma probed by the MI experiment. The effects of such perturbations on the measurements depend on how close the perturbation source is to the MI electric sensors. Thus, their impact is typically minimized by placing the sensors of the instrument far from the satellite platform by means of long deployable booms. Note that this type of perturbation is typically handled when ensuring the ElectroMagnetic Compatibility between the different sub-systems composing the satellite (Youssef, 1996).
- (ii) The spacecraft platform interacts with the plasma and triggers the formation of a plasma sheath that embeds the satellite. MI electric sensors installed near the satellite platform can be surrounded by such plasma sheath. If that is the case, the inhomogeneous plasma region embedding the sensors might modify the characteristics of MI emitted signals and, as a consequence, might affect the MI diagnostic performance. To mitigate such perturbations, MI sensors are typically installed on long booms. However, long booms cannot always be used. For instance, in the case of missions probing plasmas with large Debye lengths with respect to the size of the satellite (e.g., $\lambda_D \simeq 10$ m in the solar wind at 1 AU), sufficiently long booms might not be embarked on the spacecraft. This is also the case for nanosatellites, for which volume and mass are very constrained and long booms cannot be carried by the platform (West et al., 2015). Hence, the impact of the plasma sheath on MI measurements is not always negligible and, in some cases, cannot be ignored.
- (iii) Similarly to satellite platforms, also MI instruments interact with the surrounding plasma and get charged to a given electric potential. In response to such potential, a plasma sheath forms around MI antennas. As this plasma sheath surrounds the instrument, its impact on the measurements cannot be reduced by changing

the instrument's location. Hence, to better understand MI measurements, the instrument's self impact on the measurements needs to be accounted for. We note that the plasma sheath is expected to induce significant perturbations of the temperature diagnostic of MI measurements due to their dependency on the local characteristics of the plasma enveloping the MI sensors.

In the case of the RPC-MIP instrument onboard the Rosetta mission, the minimization of spurious electric perturbations was accomplished by installing the MI instrument on a boom of approximately 1.5 m (Carr et al., 2007) attached to the spacecraft body ($\lambda_p \approx 0.1$ m inside the coma of 67P/CG) (Gilet et al., 2017). This mitigation strategy reduced the perturbations generated by (i) electronic components onboard the satellite and by (ii) the satellite plasma sheath. But, due to their nature, perturbations caused by (iii) the instrument's plasma sheath could not be prevented and had to be taken into account. Past models of the MI instrumental response assumed a linear plasma response to MI excitation signal, a homogeneous plasma and negligible transient effects (Geiswiller et al., 2001; Gilet et al., 2017). Hence, they could not be used for investigating the impact of the plasma sheath on RPC-MIP measurements. This issue was investigated by Wattiaux et al. (2019, 2020), that obtained the instrumental response of RPC-MIP by modeling the plasma sheath embedding the instrument as a step-like vacuum sheath surrounding the sensors.

Similar investigations will be required for future MI space applications, where significant perturbations of MI measurements related to the presence of the plasma sheath are expected. This is the case for the PWI-AM2P instrument onboard the Mio spacecraft of the BepiColombo mission. PWI-AM2P uses two emitting and two receiving electric antennas installed on four 15 m wires (Karlsson et al., 2020) and the local Debye length is expected to range between 1 and 10 m in Mercury's magnetosphere (Kasaba et al., 2010). Hence, Debye length encountered by PWI-AM2P is not always expected to be negligible with respect to the distance between MI electric sensors. It results that the PWI-AM2P deployable wires cannot always ensure negligible (ii) perturbations of PWI-AM2P measurements caused to the satellite plasma sheath. Therefore, the impact of the plasma sheath on the measurements will need to be accounted for. We note that the effect of the plasma sheath is not expected to be negligible also for the RPWI-MIME MI experiment onboard the JUICE ESA mission, which launch is scheduled for April 2023. RPWI-MIME will investigate the ionospheric environment of Jupiter's moons, among which Ganymede, where the Debye length is expected to range from about 1 m to about 10 m between 200 and 500 km of altitude. Such Debye lengths are not negligible with respect to the distance between the sensor and the satellite platform (i.e., 3 m) or to the emitting-receiving electric sensors distance of the instrument (i.e., about 5–10 m). As a consequence, the impact of the plasma sheath on the measurements of RPWI-MIME onboard JUICE needs to be taken into account.

In all, the procedure used by Wattiaux et al. (2020) in the case of RPC-MIP provides an accurate instrumental response for specific plasma inhomogeneities surrounding the antennas. Indeed, such an approach is extremely efficient and can be used to improve our understanding of MI measurements for any specific space application (e.g., PWI-AM2P onboard BepiColombo). However, due to its dependence on the measurements, it provides an understanding of the plasma sheath's effects that is specific to certain MI space applications. To support future MI instruments, in this study we focus on the general impact that local space charge inhomogeneities compatible with the (ii) satellite's and (iii) instrument's plasma sheath have on MI experiments, independently of the particular geometric configuration of the MI antennas or of the satellite platform.

While the effect of small-scale (i.e., of the order of the Debye length) plasma inhomogeneities on MI measurements is unknown, wave propagation over large-scale inhomogeneities (i.e., wavelength small with respect to the inhomogeneity's size) is a topic extensively investigated by different authors (e.g., Krasnoselskikh et al., 2019; Tkachenko et al., 2021). The equations describing the evolution of electric waves along large-scale inhomogeneities are referred to as Wentzel-Kramers-Brillouin (WKB) solutions (Brillouin, 1926; Kramers, 1926; Wentzel, 1926), in honor of those that devised the method. WKB solutions show that propagating electromagnetic waves crossing large-scale plasma inhomogeneities characterized by a slowly varying refraction index (i.e. $da/\alpha \ll dz/z$ with α the refraction index and z the direction along which the plasma is inhomogeneous) react with a variation of their wavelength along the inhomogeneity as $\lambda = \lambda_0/\alpha$ with λ_0 the wavelength of the wave when propagating in the vacuum. Do the satellite's and instrument's plasma sheath have the same impact on the propagation of plasma waves such as MI emission signals?

In this context, with this investigation we aim to answer a fundamental question regarding MI experiments, which is to understand the locality of in situ MI plasma diagnostic. In particular, we want to quantify the impact

that small-scale plasma inhomogeneities with a typical size of the spacecraft plasma sheath have on MI plasma density and electron temperature diagnostic performances. For this purpose, we use a full kinetic 1D-1V cartesian Vlasov-Poisson numerical model to simulate the plasma response to MI emissions under different plasma density gradients. Note that we only consider MI experiments perturbing unmagnetized plasmas (i.e. $\omega_{ce} \ll \omega_p$).

This document is organized as follows. In Section 2, we describe the numerical model and the plasma density profiles used to numerically simulate plasma inhomogeneities at different positions with respect to MI emitting antennas. In Section 3, we show the results of our numerical simulations. In Section 4, we compare the impact on MI measurements of small-scale plasma inhomogeneities to that of large-scale inhomogeneities. In Section 5, we finalize our investigation by discussing our conclusions.

2. Full Kinetic Electrostatic 1D-1V Cartesian Vlasov-Poisson Model With Plasma Inhomogeneities

We perform numerical simulations to investigate the impact of local space charge inhomogeneities on MI measurements. We use a 1D-1V cartesian full kinetic Vlasov-Poisson model to evolve in time a box of unmagnetized, collisionless plasma perturbed by MI emission signals. The model solves the Vlasov-Poisson system of equations following the eulerian algorithm of Mangeney et al. (2002). Such numerical model has been adapted and validated in Bucciantini et al. (2022) for the investigation of the impact of large emission amplitudes on MI plasma diagnostic performance.

MI measurements are performed over time scales much shorter than ion scales. Hence, small electric field amplitudes ensure a negligible contribution of the ion dynamics to MI measurements. This allows one to simplify the model by assuming the ions as a fixed background of positive charges (i.e. $\partial f_i / \partial t = 0$) with a given density profile. Note that such assumption enables one to significantly reduce the computing resources required for performing this analysis. Thus, we only evolve in time the Vlasov equation for electrons and we neglect the ion motion by discarding the Vlasov equation for ions:

$$\frac{\partial f_e(x, t, v_e)}{\partial t} + v_e \frac{\partial f_e(x, t, v_e)}{\partial x} - \frac{e}{m_e} E \frac{\partial f_e(x, t, v_e)}{\partial v_e} = 0 \quad (1)$$

where f_e is the electron distribution function, x is the position, v_e is the electron velocity, t is the time, e is the electron charge, m_e is the electron mass and E is the electric field. The electric field influencing the motion of electrons is computed self-consistently, using the Poisson equation:

$$\frac{\partial E}{\partial x} = e \frac{n_i(x) - n_e(x, t)}{\epsilon_0} + \frac{\rho_{ext}(x, t)}{\epsilon_0} \quad (2)$$

where $n_i(x)$ is the ion density profile is considered fixed in time, $n_e(x, t)$ is the electron density and $\rho_{ext}(x, t)$ is a source term used for the simulation of MI emitting antennas. The oscillating electric charge ρ_{ext} reads:

$$\rho_{ext}(x, t) = \sigma_0 \delta(x) \sin(2\pi f t) \quad (3)$$

where σ_0 is the emission amplitude and f the emission frequency. The emission amplitude is chosen to ensure the excitation of small amplitude signals in the plasma, which are associated to a linear plasma response (i.e., $(E^2 \epsilon_0) / (n_0 k_b T_e) < 0.1$) (Bucciantini et al., 2022).

The boundary conditions of the model are periodic in physical space while, in velocity space, the distribution functions are imposed equal to zero for velocities outside a given range (i.e., $f_e(x, |v_e| > v_{max\ e}, t) = 0$, where $v_{max\ e} = 10 v_{the}$). We note that the choice of a periodic boundary condition imposes a limit on the duration of the numerical simulation so that re-entrance of plasma waves in the periodic boundary is avoided.

A periodic physical space requires the antennas to be arranged in such a way that the electric field and electric potentials are also periodic in the box. Practically, this means that for each antenna polarized with a specific electric charge we put in the box a second antenna polarized with opposite charge. This second antenna generates an electric field which is opposite to that of the first antenna. As a result, the far-field electric field (Podesta, 2005) of the two antennas is neutralized and the fields in the plasma box are periodic.

We chose to use the same geometric configuration used for a past study by Bucciantini et al. (2022) (Model B configuration). Hence, we perturb the plasma box using a succession of four emitting antennas charged with

Table 1
Parameters Defining the Simulated Inhomogeneities in Our Numerical Runs

Simulation	x_0/λ_D	L^2	A/V_0
S_00	0	1.95	± 0.5
S_01	1	1.95	± 0.5
S_02	2	1.95	± 0.5
S_04	4	1.95	± 0.5
S_08	8	1.95	± 0.5
S_16	16	1.95	± 0.5
L_50	50	4,000	± 0.5

opposite electric charge by pairs. Practically, the configuration of the antennas corresponds to that of the electrodes of two capacitors in series. The distance between two neighbor electrodes is always the same and it corresponds to one fourth of the spatial size of the numerical box.

Plasma inhomogeneities are simulated by initializing the numerical model with given electron and ion density profiles. Such profiles are obtained as follows.

First, electrons are modeled as Maxwellian:

$$\frac{n_e(x, t = 0)}{n_0} = \exp\left(\frac{V(x, t = 0)}{V_0}\right) \quad (4)$$

where $n_e(x, t)$ is the electron density, n_0 the normalization density of the numerical model corresponding to the density far from the plasma inhomogeneity, $V(x, t)$ the electric potential in the plasma, $V_0 = k_B T_e / e$ the normalization electric potential of the model, with e the electron charge, k_B the Boltzmann constant and T_e the normalization electron temperature.

Second, we impose in the numerical plasma box an initial Gaussian profile for the electric potential:

$$V(x, t = 0) = A \exp\left[-\left(\frac{x - x_0}{L\lambda_D}\right)^2\right] \quad (5)$$

where A is the amplitude of the electric potential at the center of the inhomogeneity, x_0 is the position of the plasma inhomogeneity with respect to the MI emitting antenna, L the scale of the inhomogeneity and λ_D the Debye length. We note that a positive (resp. negative) value of A corresponds to a plasma inhomogeneity with excess (resp. depletion) of electrons.

Third, we compute self-consistently the ion density profile (n_p) using the Poisson equation.

$$\nabla^2 V(x, t = 0) = -e \frac{n_p(x, t = 0) - n_e(x, t = 0)}{\epsilon_0} \quad (6)$$

We note that the numerical box is perturbed by MI signals emitted from multiple electric antennas, according to the Model B configuration discussed above. For the sake of symmetric perturbations of the plasma box, we choose to simulate plasma inhomogeneities localized at distance x_0 from each emitting antenna. It follows that a small-scale inhomogeneity at $x_0 = 0$ corresponds to a plasma inhomogeneity centered at the MI emitting antennas.

In Table 1 we list the parameters defining the plasma sheath used for initializing our numerical runs. For the numerical runs S_00 to S_16 the size of the plasma inhomogeneity is assumed small, of the order of the Debye length. For the numerical run L_50 the inhomogeneity is a localized space charge of size significantly larger than the Debye length. The density profiles used for our analysis differ from the actual solution of the 1D plasma sheath (Riemann, 1991). Such solution was discarded because it presented non-smooth density profiles at the position of the antennas, that resulted in unstable numerical runs due to the spatial periodicity of the numerical box. Hence, to ensure stable numerical runs, we use simplified inhomogeneity profiles over the same spatial scales as the plasma sheath, both in the case of positive and negative electric potential profiles (Equation 5). Figure 1 shows the electron density profile (blue line), the positive ion density profile (red line) and the electric potential profile (green line) associated to the plasma inhomogeneity S_16 (Table 1), with MI emitting antenna (E) at $x = 0$ and MI receiving antennas at d_1 and d_2 (R_1 and R_2 , respectively).

All numerical runs simulate a plasma box of length $X_{\max} = 4,000 \lambda_D$, with $n_x = 8,192$ spatial grid points. The electron distribution function is assumed non-zero for the electron velocity v_e in the range $(-10 v_{the}, 10 v_{the})$, discretized with $n_v = 101$ velocity grid points. The time-step of the numerical runs is set to $dt = 10^{-3} \omega_p^{-1}$. The amplitude of the emitted signals is $\sigma = 10^{-5} \hat{\sigma}$ with $\hat{\sigma} = en_0 \lambda_D$ the normalized amplitude of the charges at the emitting antennas. MI spectra are obtained for the frequency range $(0.5 \omega_p, 3.2 \omega_p)$ with a relative discretization of the MI spectra of $\Delta\omega/\omega_n = 0.05$. Such frequency resolution corresponds to a plasma density resolution of 10%, which is used as reference in the following section.

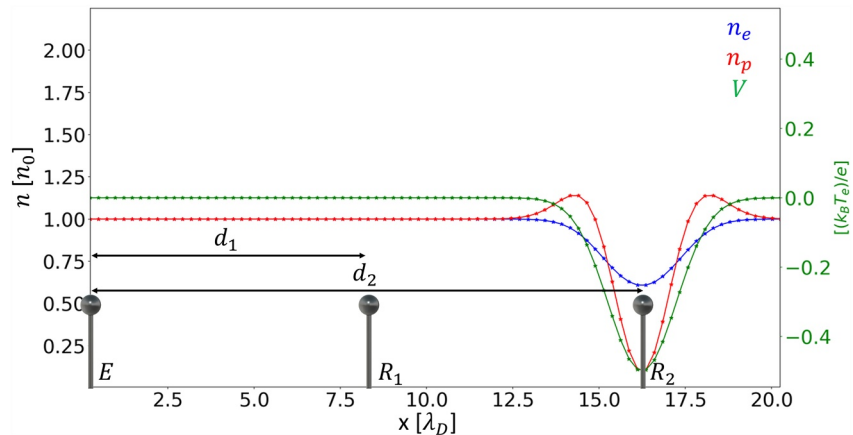


Figure 1. Example of small scale plasma inhomogeneity in correspondence of the Mutual Impedance (MI) antennas. Red and blue lines represent the positive ion and electron density profiles, respectively. The green line represents the electric potential profile associated to the density gradients. The label E at $x = 0$ represents the MI emitting antenna. The label R_1 (resp. R_2) represents the receiving antenna placed at $x = d$ (resp. $x = 2d$), in this case, $d = 8\lambda_D$ and the inhomogeneity is placed at $x_0 = 16\lambda_D$.

3. Diagnostic Performance of Mutual Impedance Experiments in the Presence of Inhomogeneous Plasma Regions

In this section, we use the 1D-1V Vlasov-Poisson model (Section 2) to investigate the diagnostic performance of MI experiments in the presence of small-scale plasma inhomogeneities (density profiles from Section 2). First, we describe MI experiments and show how MI spectra are obtained from our numerical simulations (Section 3.1). Second, we assess the impact of localized plasma inhomogeneities on both MI plasma density (Section 3.2) and electron temperature (Section 3.3) diagnostic performance.

3.1. Description and Modeling of Mutual Impedance Measurements

MI instruments consist of a set of emitting and a set of receiving electric antennas. The measurement is performed as follows. (i) The emitting antennas excite the plasma with given electric signals. Simultaneously, (ii) the receiving antennas measure the plasma electric potential fluctuations triggered by the emission. (iii) MI spectra are built from the retrieved fluctuations. Then, (iv–v) the plasma density and electron temperature are derived from the position and the shape of the resonant signatures of MI spectra, respectively. These different steps of MI measurements are modeled as follows.

- (i) MI emission signals are composed of a succession of j elementary sinusoidal signals, each oscillating at a given frequency. The i -th elementary signal (with $i = 0, \dots, j - 1$) is injected in the plasma by polarizing the emitting antennas with the electric charge σ_i that reads:

$$\sigma_i(\omega_i, t) = \sigma \sin \omega_i t \quad (7)$$

where $\omega_i = \omega_{\min}(1 + \Delta)^i$ is the i -th emitted frequency, σ the amplitude, ω_{\min} the lowest investigated frequency and Δ the frequency resolution. The signal σ_i is emitted for the duration $T_i = 2\pi N/\omega_i$, with N the amount of repetitions of the period of frequency ω_i .

In order to mimic typical MI experimental space applications such as the DFP-COMPLIMENT instrument onboard the Comet Interceptor mission, we choose both N and Δ to be the same for all emitted frequencies. In our case, we fix $N = 20$ and $\Delta = 0.05$. To such resolution corresponds a relative plasma density uncertainty of $|\Delta n_e|/n_e = 10\%$ that we use as a reference for the plasma density detection errors in the following sections. The range of investigated frequencies is $(\omega_{\min}, \omega_{\max}) = (0.5 \omega_p, 3.2 \omega_p)$ that embeds the plasma frequency ω_p .

- (ii) While the emitting antennas perturb the plasma, the receiving antennas measure its electric potential fluctuations. Such fluctuations are measured using a dipolar receiving antennas configuration. It consists of measuring the electric potential difference between two receiving antennas placed at distance d and $2d$ from the emitting antennas. Mimicking typical experimental space applications, we focus on emitting-receiving antennas distances going from $d = 0$ to $d = 30\lambda_D$.

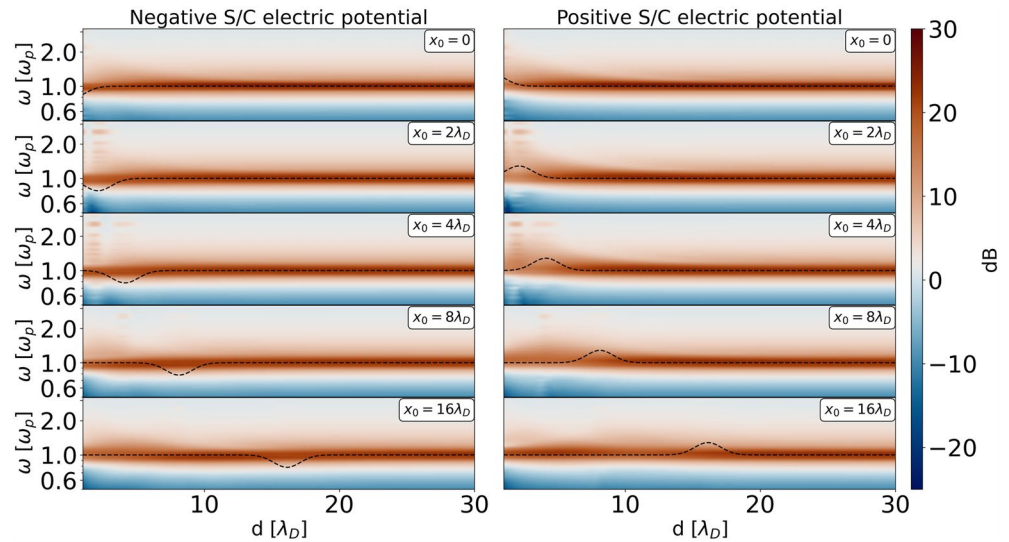


Figure 2. Mutual impedance spectra in the presence of a local space charge with negative (left panels) or positive (right panels) electric potential, in function of the emitting-receiving antennas distance d . The plasma sheath is centered at distance x_0 (Table 1) with respect to the emitting antennas. The black dashed line represents the local plasma frequency, obtained from the conversion of the electron density profile of the inhomogeneity.

(iii) MI spectra are built by computing, from the received signal, the spectral energy components corresponding to the emitted frequencies. In particular, for each emitted frequency, we compute a Discrete Fourier Transform (DFT) on the electric fluctuations measured while that frequency was being emitted. This is called a synchronous DFT analysis. Then, to highlight the response of the plasma to the emission, we mimic typical MI space applications (e.g., RPC-MIP onboard Rosetta (Trotignon et al., 2007)) and normalize each spectrum to the corresponding vacuum response (i.e., MI spectrum obtained in vacuum). Such MI spectra have resonant signatures in correspondence to the characteristic frequencies of the probed plasma (Béghin & Debric, 1972; Gilet et al., 2017; Grard, 1997; Storey et al., 1969). In the case of a negligible magnetic field, as in our investigation, the spectra have only one resonance at the plasma frequency $\omega_p = \sqrt{(e^2 n_e)/(\epsilon_0 m_e)}$, where n_e is the plasma density.

In Figure 2, we show the MI spectra in decibel (dB) scale where the reference are the corresponding measurements obtained in vacuum. Such spectra are obtained for the small-scale inhomogeneous plasmas located at different positions, as listed in Table 1 in function of the distance d between emitting and receiving antennas. Left (resp. Right) panels show the spectra obtained for the inhomogeneities associated to negative (resp. positive) electric potential profiles. The black dashed lines show the local plasma frequencies, computed using the plasma density profiles that describe the inhomogeneities (see Section 2). We observe that the resonant signature of the spectra (red colored region) does not follow the local plasma frequency variations related to the local space charge, both in the case of negative and positive electric potential profiles. Instead, it remains near ω_p which is the resonant frequency of the homogeneous plasma unperturbed by the inhomogeneity. For instance, in the left bottom panel ($x_0 = 16\lambda_D$), the resonant signature of the MI spectra does not follow the local resonant frequency variations imposed at position $d = x_0$. As discussed in Section 4, this trend is fundamentally different from what is found for MI spectra obtained for large-scale plasma inhomogeneities.

To better understand the effects that the plasma sheath has on MI measurements, we compare in Figure 3 the MI spectra obtained at specific distances from the emitting antennas (d from $5\lambda_D$ to $20\lambda_D$) and for different local space charges ($x_0 = 0, 2\lambda_D, 4\lambda_D, 8\lambda_D, 16\lambda_D$ represented with colored lines). Practically, the spectra shown in Figure 3 correspond to vertical cuts of the dynamic spectra represented in Figure 2. The reference spectra obtained for a homogeneous plasma are represented as blue lines.

Perturbations of MI measurements due to plasma inhomogeneities are essentially observed at frequencies close to the plasma frequency. However, such perturbations are significant only for spectra obtained near the position of the inhomogeneity (i.e., $d \simeq x_0$). In particular, we find negligible (resp. significant) differences between the

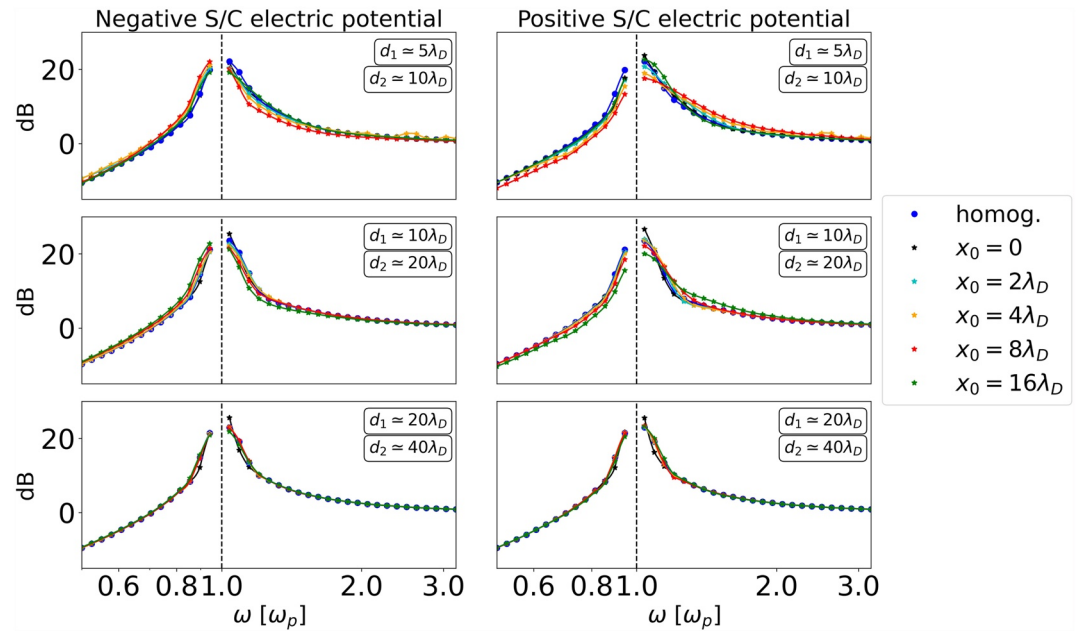


Figure 3. Examples of mutual impedance spectra obtained in the presence of the sensor/satellite plasma sheath. Left (resp. right) panels correspond to the plasma sheath of a satellite with negative (resp. positive) electric potential, placed at distance x_0 from the emitting antenna (Table 1).

perturbed spectra and the reference spectra when the receiving antennas are far from (resp. near) the inhomogeneity itself, as shown at frequency of about $1.04 \omega_p$ (resp. $0.94 \omega_p$) in the top left (resp. right) panel of Figure 3. We also find that the extent of the perturbation depends on the sign of the electric potential profile inducing the inhomogeneity. In the case of a negative (resp. positive) electric potential profile, we find that the inhomogeneity generates perturbations of the MI spectra up to 5 dB (resp. 7 dB) with respect to the reference spectra derived in the case of an homogeneous plasma. Such discrepancies are considered significant since they exceed 1 dB, which is the typical MI instrumental noise for space experimental applications (Bucciattini et al., 2022).

In the following Sections 3.2 and 3.3, we investigate the impact that the perturbations of the spectra have on the (iv) plasma density and (v) electron temperature diagnostic performance, respectively. Although they are used in a different context, we note that the procedures used in the following sections to quantify the electron density and temperature diagnostics are identical to those developed and validated in Bucciattini et al. (2022).

3.2. Plasma Density Diagnostic Performance

In this section, we quantify the MI plasma density diagnostic performance in the presence of local space charges near MI electrodes. This is performed in three successive steps.

First, we perform a quadratic interpolation of MI spectra. Past studies showed that it improves the plasma density diagnostic performance (Bucciattini et al., 2022). Second, we estimate the apparent plasma frequency ($\omega_{p,app}$) for each spectrum shown in Figure 2. We identify it as the frequency corresponding to the position of the (interpolated) resonant peak of the spectra, according to typical MI data analysis techniques (Bahnsen et al., 1988; Décréau et al., 1978; Gilet et al., 2017; Pottelette & Storey, 1981; Pottelette et al., 1975; Rooy et al., 1972; Storey et al., 1969). In particular, we compute $\omega_{p,app}$ as the position of the maximum of the resonance. We note that the apparent plasma frequency $\omega_{p,app}$ derived from the spectra might differ from the known actual plasma frequency ω_p of our numerical simulations. Third, we compare the apparent and actual plasma frequencies and compute the plasma frequency relative error:

$$\frac{\Delta\omega_p}{\omega_p} = \frac{\omega_{p,app} - \omega_p}{\omega_p} \quad (8)$$

where ω_p is the plasma frequency of the homogeneous plasma, which is equivalent to the plasma frequency far from the plasma inhomogeneity.

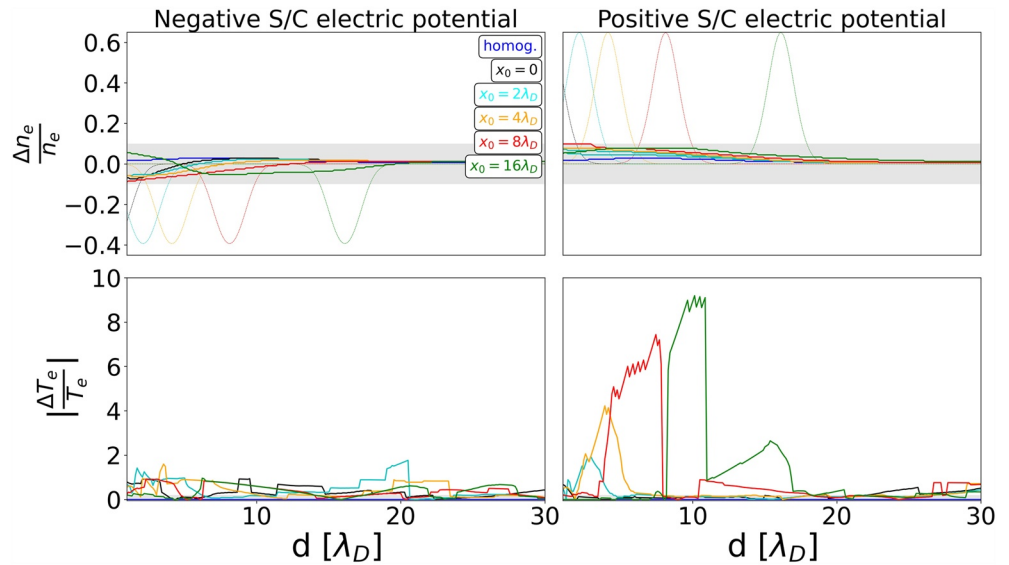


Figure 4. Plasma density (top panels) and electron temperature (bottom panels) relative errors derived from Mutual Impedance (MI) spectra in function of the distance d from the emitting antennas. Both top and bottom panels indicate the errors that one would make if the presence of local space charges near MI electrodes is neglected in the analysis. Left (resp. Right) panel: local space charge associated to negative (resp. positive) electric potential profiles. x_0 is the central position of the plasma sheath. Top panel: the gray shaded area represents the reference density uncertainty of 10%. The solid blue lines represent the relative error obtained for a homogeneous plasma. In matching colors, the solid and dashed lines represent the obtained plasma density relative error and the corresponding discrepancy between inhomogeneous density profile and reference homogeneous profile. Bottom panel: the colored lines represent the electron temperature uncertainties.

The plasma density diagnostic performance of MI experiments is, then, obtained by converting the plasma frequency relative error to plasma density relative error:

$$\frac{\Delta n_e}{n_e} = 2 \frac{\Delta \omega_{p,app}}{\omega_p} \quad (9)$$

where n_e is the density of the homogeneous plasma.

In the top panels of Figure 4, we show the plasma density relative errors obtained for local space charges induced by a negative (left panel) or positive (right panel) electric potential profiles, in function of the emitting-receiving antennas distance d . The gray shaded area represents the reference density uncertainty $\Delta n_e/n_e = 10\%$. The dashed colored lines represent the discrepancy between the density profiles of the inhomogeneous and homogeneous plasmas. Practically, the dashed lines are computed as the difference between the electron density profile and the density of the homogeneous plasma found far from the inhomogeneity. Therefore, the dashed lines show the error that would be made if the MI instrument detected the local density of the inhomogeneity. We find that plasma density relative errors (solid colored lines) are negligible, as they are always of the same order of magnitude as the reference 10% density uncertainty (gray shaded area) of the measurements. On top of that, we find that the density relative errors are negligible with respect to the difference between the inhomogeneous and homogeneous plasma density profiles (dashed lines). For instance, in the case of a local space charge due to a negative electric potential profile at $x_0 = 16\lambda_D$ (top left panel), the obtained uncertainty (green line) remains within the reference density uncertainty (gray area). The discrepancy between the reference homogeneous plasma and the inhomogeneous density profile (green dashed line), instead, significantly exceeds the error of 10%.

All in all, our results indicate that small-scale density inhomogeneities (i.e., of the order of the Debye length) compatible with plasma sheath plasma inhomogeneities have negligible impact on performance of the plasma density diagnostic provided by MI experiments.

3.3. Electron Temperature Diagnostic Performance

In this section, we quantify the impact of local space charges on the electron temperature diagnostic performance. This technique is composed of two successive steps.

First, we use the apparent plasma density $n_{e,app}$ identified from the analysis of the spectra (Section 3.2) to derive, for each MI spectrum, the ratio of the apparent Debye length $\lambda_{D,app} = \sqrt{(\epsilon_0 k_B T_{e,app}) / (e^2 n_{e,app})}$ to the actual Debye length $\lambda_D = \sqrt{(\epsilon_0 k_B T_e) / (e^2 n_e)}$. Following the same technique used by Wattiaux et al. (2020) for the analysis of RPC-MIP measurements in the case of the Rosetta mission, we compute the ratio between apparent and actual Debye lengths from the comparison between the modeled MI spectra and reference spectra obtained for a homogeneous plasma. Each reference spectrum is associated to the emitting-receiving antennas distance d_{ph} at which it is obtained. The comparison consists of computing the root-mean-squared error $\chi = \sqrt{\sum (x_i - y_i)^2 / S}$, where S is the amount of Fourier components of each MI spectrum (i.e., number of emitted frequencies), x_i and y_i are the i -th Fourier components of the observed and reference MI spectra, respectively. To mimic similar space applications of this method, the error χ is computed only after imposing the equivalence between the plasma density of the reference spectra and the apparent plasma density.

The reference spectrum associated to the minimum root-mean-squared error is called the *matching* spectrum. The matching spectrum is assumed to be the (homogeneous) equivalent of the observed (inhomogeneous) spectrum. Hence, we assume that the observed and matching spectrum are obtained for the same distance d_{app} , which is the distance for which the matching spectrum is computed. We note that such distance might differ from the actual distance d at which the observed spectrum is obtained. The relation between the apparent distance d_{app} and the actual distance d of the observed spectrum reads:

$$d_{ph} = d_{app} \lambda_{D,app} = d \lambda_D \quad (10)$$

where d_{ph} is the (non-normalized) physical distance between emitting and receiving MI antennas, which is fixed by design of the instrument. The ratio between apparent and actual distances corresponds to the ratio between the actual and apparent Debye lengths. Second, we compare the apparent and actual electron temperatures and compute the electron temperature relative error:

$$\frac{|\Delta T_{e,app}|}{T_e} = \frac{|T_e - T_{e,app}|}{T_e} = \left| 1 - \frac{T_{e,app}}{T_e} \right| \quad (11)$$

Such error represents the perturbation of the MI electron temperature diagnostic due to the presence of the satellite's plasma sheath near MI electric sensors. Taking into account the ratio between apparent and actual Debye lengths, the electron temperature relative error is computed as:

$$\frac{|\Delta T_{e,app}|}{T_e} = \left| 1 - \left(\frac{d}{d_{app}} \right)^2 \right| \quad (12)$$

Past studies found that the typical electron temperature uncertainty required for standard science objectives is of the order of 10%–30% (Décréau et al., 1978).

In the bottom panels of Figure 4, we show the electron temperature relative errors obtained for small-scale inhomogeneities with negative (left panel) and positive (right panel) electric potential profiles, in function of the distance from the antennas. In the case of the plasma sheath of a satellite with negative electric potential, we find electron temperature relative errors up to a factor 2. In the case of the plasma inhomogeneities associated to positive electric potential profiles, the error can be as large as a factor 9 depending on the position of the inhomogeneity and on the position at which the spectra are obtained. In both cases, the errors significantly exceed the reference errors of 10%–30%. This means that the spectra obtained in the presence of local space charges of the same scale as the plasma sheath of a satellite are not sufficiently similar to the spectra expected in the case of a homogeneous plasma. In those extreme cases, the shape of the MI spectra obtained in the presence of a local plasma inhomogeneity are so different from the MI spectra expected in the absence of such inhomogeneity, that the confidence level of the fit drops significantly. This means that the identified electron temperatures poorly represent the actual electron temperature in the plasma. It follows that one should not focus on the patterns of the apparent electron temperature errors shown in the bottom panels of Figure 4. Let us put ourselves in the position

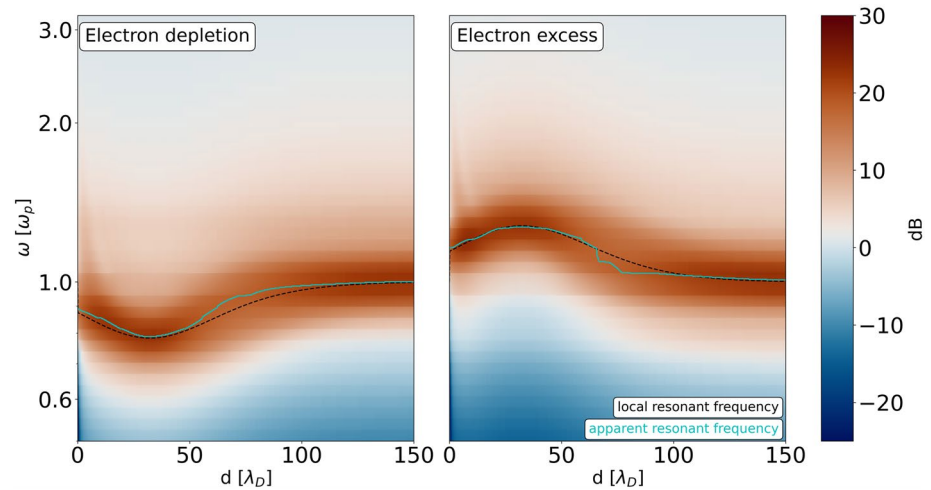


Figure 5. Mutual impedance spectra in the presence of large-scale plasma inhomogeneities, in function of the distance d . Left (resp. Right) panel obtained in the presence of inhomogeneous plasma with depletion (resp. excess) of electrons. The black dotted line represents the local plasma frequency profile associated to the local plasma inhomogeneity. The light blue line represents the apparent plasma frequency identified from the measurements.

of an observer, confronted with such data, but who ignores the presence (and the effect) of the local plasma inhomogeneity on the MI measurements. A careful observer, confronted with such discrepancies, would have certainly not concluded by providing an electron temperature that would be unacceptably false. Instead, he would have concluded that the instrument model is not compatible with the measurement: he would therefore have not provided any temperature estimations from the MI spectra. All in all, we conclude that it is not satisfactory to ignore the presence of the plasma sheath surrounding a charged spacecraft when performing electron temperature measurements using MI experiments. Instead, it is necessary to account for such local plasma inhomogeneity.

4. Mutual Impedance Spectra Obtained in the Presence of Large-Scale Plasma Inhomogeneities

We have shown that MI measurements provide the density of the plasma unperturbed by the presence of localized space charges. In particular, MI plasma density measurements are not affected by small-scale plasma density variations (e.g., satellite's plasma sheath). But, if the instruments carried by the satellite cross regions with large-scale plasma density variations, are in situ MI experiments able to retrieve the slowly varying plasma density? Large-scale plasma inhomogeneities are known to modify the properties of propagating plasma waves. In this section, we investigate for the first time what is their repercussion on MI measurements.

For this purpose, we derive MI spectra for the plasma inhomogeneity identified as L_{50} in Table 1. In particular, MI measurements are obtained both for inhomogeneities with depletion (left panel) and excess (right panel) of electrons. Figure 5 shows the MI spectra we obtained in function of the distance d . The spectra are compared to the profile of the local plasma frequency (black dashed line), which is derived from the density profile of the inhomogeneity. We remind the reader that the MI spectra investigated in this study are built using a dipolar antenna configuration. In particular, spectra at position d are obtained using the electric potential difference measured between a first antenna at $d_1 = d$ and a second antenna at $d_2 = 2d$. According to the density profile of the inhomogeneity, the local plasma density at the positions of the two antennas might differ (i.e., $n_e(x = d_1) \neq n_e(x = d_2)$). Hence, for sake of simplicity, we choose to use as reference local density the quadratic mean of the densities seen by the two antennas. The corresponding local plasma frequency is obtained from the conversion of the local plasma density (black dotted line). The apparent plasma frequency, identified as the frequency associated to the maximum of the resonant peak of the spectra, is represented as a light-blue line.

We find that both the resonant signature (red colored region) of the spectra and the apparent plasma frequency (light blue line) follow the local plasma frequency profile of the inhomogeneity (black dotted line). The discrepancy between the apparent and local plasma frequency is found up to 7%, which is of the order of the frequency

resolution of the measurement ($\Delta = 5\%$ corresponding to a density resolution of 10%). Since such apparent and local frequencies are associated to the apparent and local plasma density, our investigation indicates that MI experiments are indeed able to measure the large-scale density variations of the plasma surrounding MI electric sensors.

This result agrees with the (WKB) theory of plasma waves propagating through large-scale plasma inhomogeneities. Such theory was first devised by Wentzel, Kramers and Brillouin (Brillouin, 1926; Kramers, 1926; Wentzel, 1926). They showed that electromagnetic waves (e.g., MI emitted signals in the limit of an electrostatic plasma) propagating through stationary (i.e., over a time $\Delta t \gg 2\pi/\omega$ with ω the frequency of the wave) plasma inhomogeneities of large-scale (i.e., $\Delta z \gg \lambda$ with λ the wavelength of the wave) are perturbed as predicted by the WKB solutions:

$$E = A\alpha^{-1/2} \exp\left(\pm ik_0 \int dz \alpha\right) \quad (13)$$

where E is the amplitude of the electric field of the wave, A is a constant, $\alpha = kc/\omega$ the refractive index, $k_0 = \omega/c$ the wavenumber of the wave when propagating in vacuum and z the direction over which the plasma is inhomogeneous.

Electrostatic waves propagating through large-scale inhomogeneities with increasing (resp. decreasing) plasma density, corresponding to an increasing (resp. a decreasing) local plasma frequency, encounter a decreasing (resp. an increasing) refraction index. Thus, as the ratio between the wave's frequency and the local plasma frequency decreases (resp. increases), Landau damping on the wave decreases (resp. increases) and the wave resonates (resp. vanishes). For strong increase in plasma density, the ratio between the frequency of the wave and the local plasma frequency becomes lower than 1 and the wave is reflected. As an example, this process is similar to the reflection of radio waves in the Earth ionosphere (Westcott, 1962).

In the case of MI experiments, a succession of signals oscillating at different frequencies is injected in the plasma. Such emission perturbs the plasma and triggers oscillations at the emitted frequencies. Depending on the position of the emitted waves along the inhomogeneity, different oscillations resonate depending on the local plasma frequency. MI instruments retrieve the frequency of the resonant oscillations of the plasma. Therefore, by construction, they retrieve the local plasma frequency variations of the large-scale inhomogeneity.

Before concluding this section, it is noteworthy to remember that the WKB solutions are valid in the limit of slowly varying plasma inhomogeneities:

$$\left| \frac{3}{4} \left(\frac{1}{\alpha^2} \frac{d\alpha}{dz} \right)^2 - \frac{1}{2\alpha^3} \frac{d^2\alpha}{dz^2} \right| \ll \frac{\omega^2}{c^2}. \quad (14)$$

Therefore, the WKB solutions cannot be applied in the case of small-scale inhomogeneities (discussed in Section 3).

5. Summary and Conclusions

Spacecraft charging effects are known to impact the performances of different in situ plasma diagnostic techniques. In particular, small-scale plasma inhomogeneities (plasma sheath) triggered by the electric potential of the satellite affect both particle and wave instruments. In this context, we have investigated what is the impact of localized space charges on the performances of MI experiments, a plasma diagnostic technique used for the identification of the in situ plasma density and electron temperature. For this purpose, we have performed 1D-1V Vlasov-Poisson simulations to model MI instrumental response in the presence of plasma inhomogeneities. This study represents a first step toward understanding how local the plasma diagnostic of MI experiments is.

We find that the MI plasma density diagnostic performance is not perturbed by small-scale plasma inhomogeneities (of the order of few Debye Lengths) such as those generated in the plasma sheath of a charged spacecraft. Quantitatively, we find that the plasma density relative error does not exceed the plasma density uncertainty of 10%, which corresponds to the resolution of our measurements. This relative error decreases with the size of the emitter-receiver distance with respect to the size of the inhomogeneity. This means that MI experiments actually

retrieve the density of the unperturbed plasma away from the spacecraft sheath in which the MI sensor might be embedded. On top of that, while being unaffected by small-scale (up to few Debye lengths) inhomogeneities like the plasma sheath, we find that the plasma density diagnostic of MI experiments is able to retrieve large-scale density variations (from few tens of Debye lengths) encountered by the MI sensors (Section 4). This means that the experiment is able to measure the density gradients naturally generated in space plasmas by, for example, plasma instabilities or turbulence, down to scales of few tens of Debye lengths.

Instead, for the electron temperature diagnostic performance, we find significant discrepancies between the instrumental response obtained in the presence of the plasma sheath with respect to that expected in its absence, resulting in errors that could be up to a factor 2 (resp. 9) for measurements performed in the vicinity of a spacecraft sheath associated to a negative (resp. positive) electric charge. In both cases, the error exceeds a desired electron temperature uncertainty of 10%–30%. To mitigate the impact of the spacecraft sheath on the temperature diagnostic, one has to model the small-scale plasma inhomogeneity surrounding the instrument and/or the spacecraft when computing the reference spectra used for the derivation of the temperatures. Our results are in agreement with the work of Wattiaux et al. (2020), that has shown the necessity to account for the plasma sheath surrounding the Rosetta spacecraft and/or instrument to satisfactorily derived the electron temperatures from RPC-MIP measurements. In that study, a step-like function was used to model the plasma sheath of the negatively charged Rosetta satellite platform in the model used for computing the reference MI spectra.

From a science of measurement point of view, our study indicates that the plasma diagnostic provided by MI experiments is not strictly local. Instead, it is the result of the excitation of the plasma over a range of tens of Debye lengths surrounding the electric sensors. Consequently, MI plasma density measurements are found to be immune to the local perturbations of the plasma generated by the floating electric potential of the satellite on which MI sensors are accommodated. Moreover, our study also illustrates that MI experiments plasma density measurements, unaffected by local perturbations associated to spacecraft charging, present a crucial advantage compared to other complementary, in situ, plasma diagnostic techniques.

This result can be understood and interpreted as follows. The MI technique is essentially based on the measurement of the plasma dielectric, from which plasma diagnostics such as the electron density and temperature are retrieved. The plasma dielectric itself is based on the notion of collective behavior of charged particle in a plasma. Such collective plasma behavior only exists on scales larger than the Debye length. Practically, in an unmagnetized plasma, the features observed in MI spectra at frequencies close to the plasma frequency are associated with the generation and the propagation of Langmuir waves. Those waves carry information on scales much larger than the Debye length: therefore the MI emitter is actually exciting the plasma over a spatial range much larger than the Debye length. Those collective oscillations are actually blind to small-scale fluctuations of the order of the Debye length itself, such as the spacecraft sheath, over which they propagate undisturbed, and oscillate at the eigenfrequency of the unperturbed plasma (the plasma frequency) away from such small-scale inhomogeneity. This is why the retrieved plasma frequency is that of the unperturbed plasma away from the spacecraft sheath, and so is the plasma density diagnostic. However, for a hot plasma (i.e., for a plasma such that the Debye length is not short compared to the emitter-receiver distance of the MI experiment), the temperature diagnostic is based on the Landau damping of the generated waves. Such damping depends on the amount of charged particles, along the wave path, that can exchange energy with the generated electric signal (essentially absorb it). It can therefore directly be impacted by a local plasma inhomogeneity, especially for strongly damped Langmuir waves. This is why the temperature diagnostic depends on the local characteristics of the plasma surrounding the MI sensors.

From a practical point of view, our results will be directly useful for the PWI-AM2P experiment onboard the Mio spacecraft of the ESA-JAXA BepiColombo mission that will investigate the surroundings of Mercury. At Mercury, photoelectric effects are expected to charge positively the Mio spacecraft when in sunlight. This means that we expect, at least for a significant part of the mission, a plasma sheath characterized by a local excess of electrons. The size of such plasma sheath shall be of the order of the Debye length λ_D that is expected to be in the range 1–10 m in the plasma environment of Mercury, while the electric sensors (the MEFISTO antennas (Karlsson et al., 2020)) are 15 m long. Our investigation indicates that one has to include the plasma sheath of the Mio spacecraft in the modeling and the analysis of PWI-AM2P spectra to retrieve satisfactorily the electron temperature.

We note also that this study will be useful for all future space applications of MI experiments, among which we recall the RPWI-MIME onboard the JUICE mission (resp. the CDFP-OMPLIMENT instrument onboard Comet

Interceptor), where the local Debye length of the plasma encountered by the satellite is expected to be of the same order as the distance between RPWI-MIME (resp. DFP-COMPLIMENT) electric sensors.

Data Availability Statement

Datasets for this research are available at (Bucciantini, 2023), together with a detailed explanation on how to use them. The model used to produce such data set is described in Section 2. It is based on the model implemented by Mangeney et al. (2002). The 1D-1V Vlasov-Poisson version of the model, which corresponds to the one we use in our investigation, is described in Henri et al. (2010).

Acknowledgments

The work performed at LPC2E is supported by CNES APR. The Scientific color map “lajolla” (Crameri, 2021) is used in this study to prevent visual distortion of the data and exclusion of readers with color-vision deficiencies (Crameri et al., 2020). We benefited from the computing resources provided by CaSciModOT. This work was granted access to the HPC/AI resources of TGCC under the allocation 2021-A0100412428 made by GENCI. L.B. was supported by funds from Région Centre Val de Loire (France).

References

- Allen, J. E. (2008). The plasma–sheath boundary: Its history and Langmuir’s definition of the sheath edge. *Plasma Sources Science and Technology*, 18(1), 014004. <https://doi.org/10.1088/0963-0252/18/1/014004>
- Bahnens, A., Jespersen, M., Ungstrup, E., Pottelette, R., Malingre, M., Decreau, P. M. E., et al. (1988). First VIKING results: High frequency waves. *Physica Scripta*, 37(3), 469–474. <https://doi.org/10.1088/0031-8949/37/3/032>
- Béghin, C., & Debrie, R. (1972). Characteristics of the electric field far from and close to a radiating antenna around the lower hybrid resonance in the ionospheric plasma. *Journal of Plasma Physics*, 8(3), 287–310. <https://doi.org/10.1017/S002237780007157>
- Benkhoff, J., Murakami, G., Baumjohann, W., Besse, S., Bunce, E., Casale, M., et al. (2021). Bepicolombo—Mission overview and science goals. *Space Science Reviews*, 217(8), 90. <https://doi.org/10.1007/s11214-021-00861-4>
- Bergman, S., Stenberg Wieser, G., Wieser, M., Johansson, F. L., & Eriksson, A. (2020). The influence of spacecraft charging on low-energy ion measurements made by RPC-ICA on Rosetta. *Journal of Geophysical Research: Space Physics*, 125(1), e2019JA027478. <https://doi.org/10.1029/2019JA027478>
- Brillouin, L. (1926). La nouvelle mécanique atomique. *Journal de Physique et le Radium*, 7(5), 135–160. <https://doi.org/10.1051/jphysrad:0192600705013500>
- Bucciantini, L. (2023). 1D-1V Vlasov-Poisson simulations of mutual impedance experiments in the presence of small-scale and large-scale plasma inhomogeneities—Part 3. Zenodo. <https://doi.org/10.5281/zenodo.8119856>
- Bucciantini, L., Henri, P., Wattiaux, G., Califano, F., Vallières, X., & Randriamboarison, O. (2022). In situ space plasma diagnostics with finite amplitude active electric experiments: Non-linear plasma effects and instrumental performance of mutual impedance experiments. *Journal of Geophysical Research: Space Physics*, 127(12), e2022JA030813. <https://doi.org/10.1029/2022JA030813>
- Carr, C., Cupido, E., Lee, C. G. Y., Balogh, A., Beek, T., Burch, J. L., et al. (2007). RPC: The Rosetta plasma consortium. *Space Science Reviews*, 128(1–4), 629–647. <https://doi.org/10.1007/s11214-006-9136-4>
- Crameri, F. (2021). *Scientific color maps*. Zenodo. <https://doi.org/10.5281/zenodo.5501399>
- Crameri, F., Shephard, G. E., & Heron, P. J. (2020). The misuse of color in science communication. *Nature Communications*, 11(1), 5444. <https://doi.org/10.1038/s41467-020-19160-7>
- Décreau, P. M. E., Béghin, C., & Parrot, M. (1978). Electron density and temperature, as measured by the mutual impedance experiment on board geos-1. *Space Science Reviews*, 22(5), 581–595. <https://doi.org/10.1007/BF00223942>
- Geiswiller, J., Béghin, C., Kolesnikova, E., Lagoutte, D., Michau, J., & Trotignon, J. (2001). Rosetta spacecraft influence on the mutual impedance probe frequency response in the long Debye length mode. *Planetary and Space Science*, 49(6), 633–644. [https://doi.org/10.1016/S0032-0633\(00\)00173-2](https://doi.org/10.1016/S0032-0633(00)00173-2)
- Gilet, N., Henri, P., Wattiaux, G., Cilibrasi, M., & Béghin, C. (2017). Electrostatic potential radiated by a pulsating charge in a two-electron temperature plasma. *Radio Science*, 52(11), 1432–1448. <https://doi.org/10.1002/2017RS006294>
- Grard, R. (1997). Influence of suprathermal electrons upon the transfer impedance of a quadrupolar probe in a plasma. *Radio Science*, 32(3), 1091–1100. <https://doi.org/10.1029/97RS00254>
- Grard, R., Knott, K., & Pedersen (1983). Spacecraft charging effects. *Space Science Reviews*, 34(3), 289–304. <https://doi.org/10.1007/BF00175284>
- Henri, P., Califano, F., Briand, C., & Mangeney, A. (2010). Vlasov-Poisson simulations of electrostatic parametric instability for localized Langmuir wave packets in the solar wind. *Journal of Geophysical Research*, 115(A6), A06106. <https://doi.org/10.1029/2009JA014969>
- Johansson, F. L., Eriksson, A. I., Vigren, E., Bucciantini, L., Henri, P., Nilsson, H., et al. (2021). Plasma densities, flow, and solar EUV flux at comet 67P. *Astronomy & Astrophysics*, 653(4), A128. <https://doi.org/10.1051/0004-6361/202039959>
- Karlsson, T., Kasaba, Y., Wahlund, J.-E., Henri, P., Bylander, L., Puccio, W., et al. (2020). The MEFISTO and WPT electric field sensors of the plasma wave investigation on the BepiColombo Mio spacecraft. *Space Science Reviews*, 216(8), 132–216. <https://doi.org/10.1007/s11214-020-00760-0>
- Kasaba, Y., Bougeret, J. L., Blomberg, L., Kojima, H., Yagitani, S., Moncuquet, M., et al. (2010). The plasma wave investigation (PWI) onboard the BepiColombo/MMO: First measurement of electric fields, electromagnetic waves, and radio waves around mercury. *Planetary and Space Science*, 58(1), 238–278. <https://doi.org/10.1016/j.jps.2008.07.017>
- Kasaba, Y., Kojima, H., Moncuquet, M., Wahlund, J., Yagitani, S., Sahraoui, F., et al. (2020). Plasma Wave Investigation (PWI) aboard Bepi-Colombo Mio on the trip to the first measurement of electric fields, electromagnetic waves, and radio waves around Mercury. *Space Science Reviews*, 216(65), 65. <https://doi.org/10.1007/s11214-020-00692-9>
- Kramers, H. A. (1926). Wellenmechanik und halbzahlige quantisierung. *Zeitschrift für Physik*, 39(10–11), 828–840. <https://doi.org/10.1007/BF01451751>
- Krasnoselskikh, V., Voshchepynets, A., & Maksimovic, M. (2019). On the efficiency of the linear-mode conversion for generation of solar type iii radio bursts. *The Astrophysical Journal*, 879(1), 51. <https://doi.org/10.3847/1538-4357/ab22bf>
- Laframboise, J. G. (1966). Theory of spherical and cylindrical Langmuir probes in a collisionless, Maxwellian plasma at rest.
- Lai, S. T. (2012). *Fundamentals of spacecraft charging*. Princeton University Press. <https://doi.org/10.1515/9781400839094>
- Mangeney, A., Califano, F., Cavazzoni, C., & Travnicek, P. (2002). A numerical scheme for the integration of the Vlasov-Maxwell system of equations. *Journal of Computational Physics*, 179(2), 495–538. <https://doi.org/10.1006/jcp.2002.7071>
- Marchand, R., Burchill, J. K., & Knudsen, D. J. (2010). Modelling electrostatic sheath effects on swarm electric field instrument measurements. *Space Science Reviews*, 156(1–4), 73–87. <https://doi.org/10.1007/s11214-010-9735-y>

- Miyake, Y., & Usui, H. (2016). Particle-in-cell modeling of spacecraft-plasma interaction effects on double-probe electric field measurements. *Radio Science*, 51(12), 1905–1922. <https://doi.org/10.1002/2016RS006095>
- Podesta, J. J. (2005). Spatial Landau damping in plasmas with three-dimensional k distributions. *Physics of Plasmas*, 12(5). <https://doi.org/10.1063/1.188547>
- Pottelette, R., Rooy, B., & Fiala, V. (1975). Theory of the mutual impedance of two small dipoles in a warm isotropic plasma. *Journal of Plasma Physics*, 14(2), 209–243. <https://doi.org/10.1017/S0022377800009533>
- Pottelette, R., & Storey, L. R. O. (1981). Active and passive methods for the study of non-equilibrium plasmas using electrostatic waves. *Journal of Plasma Physics*, 25(2), 323–350. <https://doi.org/10.1017/S0022377800023151>
- Riemann, K. U. (1991). The Bohm criterion and sheath formation. *Journal of Physics D: Applied Physics*, 24(4), 493–518. <https://doi.org/10.1088/0022-3727/24/4/001>
- Riemann, K.-U. (2008). Plasma and sheath. *Plasma Sources Science and Technology*, 18(1), 014006. <https://doi.org/10.1088/0963-0252/18/1/014006>
- Rooy, B., Feix, M. R., & Storey, L. R. O. (1972). Theory of a quadrupolar probe for a hot isotropic plasma. *Plasma Physics*, 14(3), 275–300. <https://doi.org/10.1088/0032-1028/14/3/005>
- Snodgrass, C., & Jones, G. H. (2019). The European Space Agency's comet interceptor lies in wait. *Nature Communications*, 10(5418), 5418. <https://doi.org/10.1038/s41467-019-13470-1>
- Storey, L., Aubry, L., & Meyer, P. (1969). Mutual impedance techniques for space plasma measurements. In *Measurement techniques in space plasmas—Fields* (Vol. 103, p. 155). *Geophysical monograph series*. <https://doi.org/10.1029/GM103p0155>
- Taylor, M. G. G. T., Altobelli, N., Buratti, B. J., & Choukroun, M. (2017). The Rosetta mission orbiter science overview: The comet phase. *Philosophical Transactions of the Royal Society A: Mathematical, Physical & Engineering Sciences*, 375(2097), 20160262. <https://doi.org/10.1098/rsta.2016.0262>
- Tkachenko, A., Krasnoselskikh, V., & Voshchepynets, A. (2021). Harmonic radio emission in randomly inhomogeneous plasma. *The Astrophysical Journal*, 908(2), 126. <https://doi.org/10.3847/1538-4357/abd2bd>
- Tonks, L., & Langmuir, I. (1929). A general theory of the plasma of an arc. *Physics Reviews*, 34(6), 876–922. <https://doi.org/10.1103/PhysRev.34.876>
- Trotignon, J., Béghin, C., Lagoutte, D., Michau, J., Matsumoto, H., Kojima, H., et al. (2006). Active measurement of the thermal electron density and temperature on the Mercury Magnetospheric Orbiter of the BepiColombo mission. *Advances in Space Research*, 38(4), 686–692. <https://doi.org/10.1016/j.asr.2006.03.031>
- Trotignon, J., Michau, J. L., Lagoutte, D., Chabassière, M., Chalumeau, G., Colin, F., et al. (2007). RPC-MIP: The mutual impedance probe of the Rosetta plasma consortium. *Space Science Reviews*, 128(1–4), 713–728. <https://doi.org/10.1007/s11214-006-9005-1>
- Wattiaux, G., Gilet, N., Henri, P., Vallières, X., & Bucciattini, L. (2019). RPC-MIP observations at comet 67P/Churyumov-Gerasimenko explained by a model including a sheath and two populations of electrons. *Astronomy & Astrophysics*, 630, A41. <https://doi.org/10.1051/0004-6361/201834872>
- Wattiaux, G., Henri, P., Gilet, N., Vallières, X., & Deca, J. (2020). Plasma characterization at comet 67P between 2 and 4 AU from the Sun with the RPC-MIP instrument. *Astronomy & Astrophysics*, 638, A124. <https://doi.org/10.1051/0004-6361/202037571>
- Wentzel, G. (1926). Eine verallgemeinerung der quantenbedingungen für die zwecke der wellenmechanik. *Zeitschrift für Physik*, 38(6–7), 518–529. <https://doi.org/10.1007/BF01397171>
- West, S. T., White, C., Celestino, C., Philpott, S., & Pankow, M. (2015). Design and testing of deployable carbon fiber booms for cubesat non-gossamer applications. In *56th AIAA/ASCE/AHS/ASC structures, structural dynamics, and materials conference*. <https://doi.org/10.2514/6.2015-0206>
- Westcott, B. (1962). Ionospheric reflection processes for long radio-waves—I. *Journal of Atmospheric and Terrestrial Physics*, 24(5), 385–399. [https://doi.org/10.1016/0021-9169\(62\)90233-7](https://doi.org/10.1016/0021-9169(62)90233-7)
- Youssef, E. (1996). ECSS—European cooperation for space standardization. In *Space programs and technologies conference*. <https://doi.org/10.2514/6.1996-4305>